

Simultaneously sparse and low-rank abundance matrix estimation for hyperspectral image unmixing

Paris V. Giampouras, Konstantinos E. Themelis,

Athanasios A. Rontogiannis, *Member, IEEE*, and Konstantinos D. Koutroumbas

Abstract

In a plethora of applications dealing with inverse problems, e.g. in image processing, social networks, compressive sensing, biological data processing etc., the signal of interest is known to be structured in several ways at the same time. This premise has recently guided the research to the innovative and meaningful idea of imposing multiple constraints on the parameters involved in the problem under study. For instance, when dealing with problems whose parameters form sparse and low-rank matrices, the adoption of suitably combined constraints imposing sparsity and low-rankness, is expected to yield substantially enhanced estimation results. In this paper, we address the spectral unmixing problem in hyperspectral images. Specifically, two novel unmixing algorithms are introduced, in an attempt to exploit both spatial correlation and sparse representation of pixels lying in homogeneous regions of hyperspectral images. To this end, a novel convex mixed penalty term is first defined consisting of the sum of the weighted ℓ_1 and the weighted nuclear norm of the abundance matrix corresponding to a small area of the image determined by a sliding square window. This penalty term is then used to regularize a conventional quadratic cost function and impose simultaneously sparsity and row-rankness on the abundance matrix. The resulting regularized cost function is minimized by a) an incremental proximal sparse and low-rank unmixing algorithm and b) an algorithm based on the alternating minimization method of multipliers (ADMM). The effectiveness of the proposed algorithms is illustrated in experiments conducted both on simulated and real data.

P. V. Giampouras, K. E. Themelis, A. A. Rontogiannis and K. D. Koutroumbas are with the Institute for Astronomy, Astrophysics, Space Applications and Remote Sensing (IAASARS), National Observatory of Athens, I. Metaxa & Vas. Pavlou str., GR-15236, Penteli, Greece (e-mail: parisg@noa.gr; themelis@noa.gr; tronto@noa.gr; koutroum@noa.gr).

Index Terms

Semi-supervised spectral unmixing, hyperspectral images, simultaneously sparse and low-rank matrices, proximal methods, alternating direction method of multipliers (ADMM), abundance estimation

I. INTRODUCTION

Spectral unmixing (SU) of hyperspectral images (HSIs) has attracted considerable attention in recent years both in research and applications. SU can be considered as the process of a) identifying the spectral signatures of the materials (*endmembers*) whose mixing generates the (so called *mixed*) pixels of an HSI and b) deriving their corresponding fractions (*abundances*) in the formation of each HSI pixel, [1]. The latter constitute the so called *abundance vectors*. This two step procedure has given rise to a plethora of methods tackling either one or both these two tasks. Diverse statistical and geometrical approaches have been lately put forward in literature addressing the first step, commonly known as endmembers' extraction (e.g. [2], [3]). On the other hand, there have been many research works that assume that the spectral signatures of the endmembers are available and focus on the abundance estimation task. Algorithms that fall into this class, need to make a fundamental assumption concerning the inherent mixing process that generates the spectral signatures of the HSI pixels.

In view of the latter, the linear mixing model (LMM) holds a dominant position being widely adopted in numerous state-of-the-art unmixing algorithms (e.g. [1] and the references therein). More specifically, these algorithms are based on the premise that the pixels' spectral signatures are generated by a linear combination of endmembers' spectra contained in a predefined set, usually termed as *endmembers' dictionary*. Abundance estimation is henceforth treated as a linear regression problem. LMM has prevailed over other approaches, due to its simplicity and mathematical tractability. Physical considerations that naturally arise, impose various constraints on the unmixing problem. In this context, the so-called *abundance nonnegativity* and *the abundance sum-to-one* constraints are usually adopted. That said, unmixing can be viewed as a constrained linear regression problem.

In an attempt to achieve better abundance estimation results, recent novel ideas promote the incorporation of further prior knowledge in the unmixing problem. In light of this, several methods bring into play the *sparsity* assumption, [4]–[7]. Its adoption is justified by the fact that

only a few of the available endmembers participate in the formation of a given pixel, especially in the case of large size endmembers' dictionaries. Put it in other terms, it is envisaged that pixels' spectral signatures accept sparse representations with respect to a given endmembers' dictionary. Furthermore, one could also say that the abundance vectors corresponding to the pixels of HSIs are deemed having only a few non-zero values. Practically speaking, sparsity is imposed on abundances by means of ℓ_1 norm regularization, [4]–[6] when a deterministic approach is followed. On the other hand, in Bayesian schemes appropriate sparsity inducing priors are placed on the abundance vectors, [7], [8]. *Spatial correlation* is another constraint that has recently been incorporated in the unmixing process, offering stimulating results, [9]–[11]. In that vein, the additional information that exists in homogeneous regions of HSIs is subject to exploitation. Actually, in such regions, there is a high degree of correlation among the spectral signatures of neighboring pixels. It is hence anticipated that there should also be correlation among the abundance vectors corresponding to these pixels. This has led to the development of novel unmixing schemes, whereby the information provided by the neighboring pixels is taken into account in the abundance estimation process of each single pixel.

In this spirit, a collaborative deterministic scheme, termed CLSUnSAL, was recently proposed in [11], which uses a wealth of information stemming from all the pixels of the examined HSI. CLSUnSAL adopts dictionaries consisting of a large amount of endmembers. Then it assumes, that spatial correlation translates into abundance vectors sharing the same support set i.e., presenting a similar sparsity pattern. Thus, the matrix whose columns are the abundance vectors of all HSI pixels (called *abundance matrix*) should meaningfully be of a joint-sparse structure ¹. To impose joint-sparsity, CLSUnSAL applies a ℓ_2/ℓ_1 norm on the sought abundance matrix, which is then used to penalize a suitably defined quadratic cost function. Minimization of the resulting regularized cost function is performed by an alternating direction method of multipliers (ADMM), [13]. A similar perspective is followed in [10], however in a “localized” fashion. Specifically, [10] proposes the use of a 3×3 square window that slides all over the image. The abundance vector of the central pixel is then inferred, by taking into account the spectral signatures of the adjacent pixels contained in the window. Based on this idea, two algorithms are derived. First the MMV-ADMM, which in a similar to CLSUnSAL fashion, seeks joint-sparse

¹A joint-sparse Bayesian unmixing scheme has been also presented in [12].

abundance matrices utilizing the ℓ_2/ℓ_1 norm, and second the LRR algorithm that promotes a low-rank structure on the abundance matrix. Actually, the LRR algorithm presents an alternative way of modelling the spatial correlation among neighboring pixels. That is, it assumes that the correlation among pixels' spectral signatures can be represented by abundance vectors that are linearly dependent. Apparently, the matrix formed by these abundance vectors should be of low rank. That said, a nuclear norm is imposed on the abundance matrix, and a properly adapted augmented Lagrangian cost function is minimized in an alternating minimization fashion.

In this paper, we introduce a novel idea for performing abundance estimation in HSIs under the LMM, that takes simultaneously into consideration spatial correlation and sparsity. Similarly to [10], we utilize a $\kappa \times \kappa$ square sliding window with κ odd, that contains the spectral signatures of adjacent pixels lying in it. Departing from the usual paradigm, we propose to seek κ^2 -column abundance matrices that are *simultaneously sparse and low-rank*. SU is thus formulated as a *sparse reduced-rank regression* problem, [14]. As stated earlier, low-rankness arises naturally in abundance matrices corresponding to relatively homogeneous regions, due to the linear dependence of the respective abundance vectors. At the same time, sparsity is a reasonable hypothesis that still holds independently, as explained above, in each individual abundance vector. Broadly speaking, imposing multiple structures on the same mathematical object when dealing with inverse problems, is a strategy still in its very infancy in signal processing and machine learning literature, [15]–[17]. The aforementioned sparsity and low-rank constraints give rise to a mixed penalty term that regularizes a least squares fitting function through the weighted ℓ_1 norm and the weighted trace norm of the abundance matrices, respectively. Then, two novel iterative algorithms are proposed to minimize the resulting cost function, namely the incremental proximal sparse low-rank unmixing algorithm (IPSpLRU) and the alternating direction sparse and low-rank unmixing algorithm (ADSpLRU). As implied by their names, IPSpLRU is based on proximal operators of the individual terms that compose the cost function. On the other hand, ADSpLRU is an ADMM based approach properly adapted to our problem formulation. The proposed algorithms are compared with state-of-the-art unmixing techniques and their effectiveness is demonstrated via extensive simulated and real-data experiments.

Notation: Matrices are represented as boldface uppercase letters, e.g., \mathbf{X} , and, column vectors as boldface lowercase letters, e.g., \mathbf{x} , while the i -th component of vector \mathbf{x} is denoted by x_i and the ij -th element of matrix \mathbf{X} by x_{ij} . Moreover, T denotes transposition, \mathbf{I}_N is the $N \times N$ identity

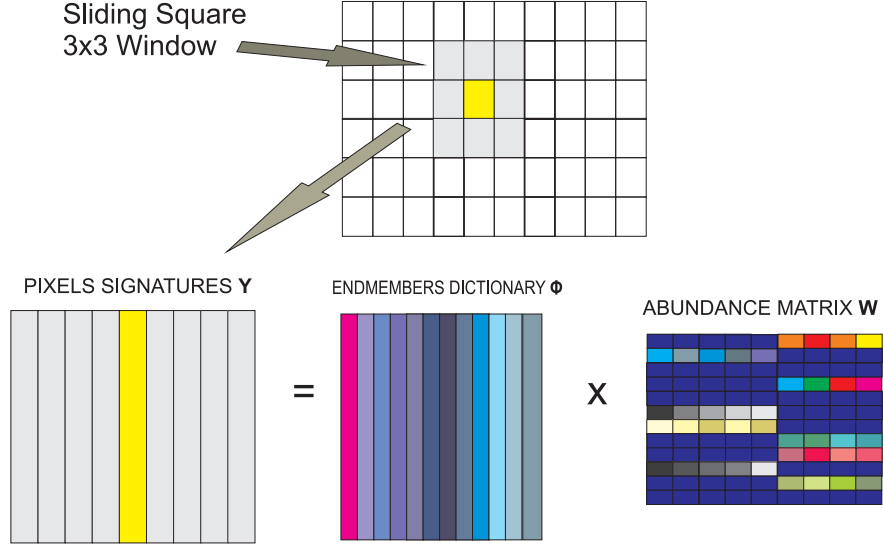


Fig. 1: Graphical illustration of the sliding window approach of our unmixing algorithms. Abundance matrix is considered sparse and low-rank (in this example rank = 2). Blue cells in matrix \mathbf{W} represent zero values.

matrix and $\mathbf{0}$ is a zero matrix with respective dimensions, $\mathbf{1}$ denotes the all ones vector, $\text{rank}(\mathbf{X})$ is the rank of \mathbf{X} , $\text{tr}[\mathbf{X}]$ denotes the trace of matrix \mathbf{X} , ∇ denotes the gradient, $\text{diag}(\mathbf{x})$ is a diagonal matrix with the elements of vector \mathbf{x} on its diagonal, $\sigma_i(\mathbf{X})$ is the i th largest singular value of \mathbf{X} , $\|\cdot\|_2$ is the standard ℓ_2 (Euclidean) vector norm, $\|\mathbf{X}\|_* = \text{Tr}(\mathbf{X}^T \mathbf{X}) = \sum_{k=1}^{\text{rank}(\mathbf{X})} \sigma_k(\mathbf{X})$, denotes the nuclear norm, $\|\mathbf{X}\|_1 = \sum_i \sum_j |x_{ij}|$ is the sum of the absolute values of all entries of \mathbf{X} (called the ℓ_1 norm), $\|\mathbf{X}\|_F = \sqrt{\sum_i \sum_j x_{ij}^2}$, stands for the Frobenius norm. $\mathcal{N}(\cdot)$ denotes the Gaussian distribution. Also, \mathbb{R}^k stands for the k -dimensional Euclidean space and \mathbb{R}_+^k denotes the k -dimensional non-negative orthant. The matrix inequality $\mathbf{X} \geq \mathbf{Y}$ declares element-wise operation and \odot stands for component-wise multiplication.

II. PROBLEM FORMULATION

We consider an L -spectral band hyperspectral image that is composed of N endmembers. Let $\Phi = [\phi_1, \phi_2, \dots, \phi_N]$ stand for the $L \times N$ endmembers' dictionary, where $\phi_i \in \mathbb{R}_+^L, i = 1, 2, \dots, N$, is the spectral signature of the i th endmember. Consider also a small sliding square window that contains the measurement spectra $\mathbf{y}_k, k = 1, 2, \dots, K$, of K adjacent pixels ($K = \kappa \times \kappa$) that are assumed to share the same endmember matrix Φ , as shown graphically in Fig.

1 for $K = 9$. In matrix notation, let $\mathbf{Y} = [\mathbf{y}_1, \mathbf{y}_2, \dots, \mathbf{y}_K]$ be the $L \times K$ matrix containing the spectra of the K selected pixels as its columns. Utilizing the linear mixing model (LMM), the mixing process can be described by the equation

$$\mathbf{Y} = \Phi \mathbf{W} + \mathbf{E}, \quad (1)$$

where $\mathbf{W} \in \mathbb{R}_+^{N \times K}$ is the abundance matrix whose columns are the N -dimensional abundance vectors of the corresponding K pixels, and $\mathbf{E} \in \mathbb{R}^{L \times K}$ is an i.i.d., zero-mean Gaussian noise matrix. Due to physical considerations, the abundance coefficients in \mathbf{W} should satisfy two constraints, namely, the *abundance nonnegativity* and the *abundance sum-to-one* constraints, [18], i.e.,

$$\mathbf{W} \geq \mathbf{0}, \text{ and } \mathbf{1}^T \mathbf{W} = \mathbf{1}^T. \quad (2)$$

Nevertheless, in the following we relax the sum-to-one constraint for the reasons explained in [6]. That said, the general problem considered in this paper is the following: “given the spectral measurements \mathbf{Y} and the endmember matrix Φ , estimate the abundance matrix \mathbf{W} subject to the nonnegativity constraint”. This is a typical inverse problem, which has been addressed via many methods in the signal processing literature. However, the efficacy of the proposed approach lies on the exploitation of the intrinsic structural characteristics of \mathbf{W} , i.e., sparsity and low-rankness. To this end, we impose concurrently two naturally justified *structural constraints* on the abundance matrix \mathbf{W} , that promote *low-rankness* and *sparsity*.

Low-rankness property: A logical consideration is that all pixels belonging to the same window are correlated, i.e., they are composed of the same materials, although maybe in different proportions. This property suggests that the abundance matrix to be estimated is either low-rank, or it can be well-approximated by a low-rank matrix. In the bibliography, low-rank matrix estimation techniques have recently emerged as powerful estimation tools, e.g., [10], [19]–[21]. These estimators are mainly based on regularization by the nuclear norm of \mathbf{W} (otherwise called the trace norm). A similar regularization is also adopted in this paper in order to impose the low-rank constraint.

Sparsity property: Another typical assumption is that only a small portion of the N endmembers will be present in the spatial area marked each time by the $\kappa \times \kappa$ shifting window. In other words, it is safe to assume that the abundance matrix \mathbf{W} has a *sparse representation* in terms

of the endmember matrix dictionary Φ . This motivates the use of a sparsity-cognizant estimator for the abundance matrix \mathbf{W} , which is envisaged to produce more robust unmixing results. It should be noted that sparsity has already been successfully exploited in many spectral unmixing algorithms, e.g., [5]–[8], [11], [22].

It is worth mentioning that the sparsity of \mathbf{W} does by no means invalidate its low-rankness. On the contrary, both structural hypotheses on \mathbf{W} are assumed to hold *simultaneously*, although low-rankness implicitly imposes some kind of structure on sparsity. So far, reports in the spectral unmixing literature explore either the sparsity, e.g. [7], [22], or the low-rankness property of \mathbf{W} , e.g. [10]. This is the first time, to our knowledge, that spectral unmixing is formulated as a simultaneously sparse and low-rank matrix estimation problem. That is, we seek a matrix \mathbf{W} that, apart from fitting the data well in the least squares sense, it has minimum rank and only a few positive elements. To achieve this, we define the following optimization problem, [15],

$$(P1) : \hat{\mathbf{W}} = \underset{\mathbf{W} \in \mathbb{R}_+^{N \times K}}{\operatorname{argmin}} \left\{ \frac{1}{2} \|\mathbf{Y} - \Phi \mathbf{W}\|_F^2 + \gamma \|\mathbf{W}\|_1 + \tau \|\mathbf{W}\|_* \right\} \quad (3)$$

where $\gamma, \tau \geq 0$ are parameters that control the trade-off between the sparsity and rank regularization terms and the data fidelity term. Being parameterized, (P1) becomes flexible enough to impose either one of the two structures on \mathbf{W} . For example, by setting $\gamma = 0$, (P1) results in recovering a matrix that has only a low-rank structure. Accordingly, setting $\tau = 0$ is tantamount to estimating a sparse matrix. The flexibility of the proposed model provides certainly an advantage over either low-rank or sparse estimation methods, as it will also be demonstrated later, in the experimental results section.

It is also worth pointing out that the convex surrogates of the zero norm $\|\mathbf{W}\|_0$ and $\operatorname{rank}(\mathbf{W})$ have been used in (P1), i.e., the ℓ_1 and the nuclear norm, respectively. In an attempt to promote further the robustness and consistency of the proposed estimator, we propose to use *weighted* ℓ_1 and nuclear norms in (P1). Such an approach is expected to enhance the sparsity of the individual elements w_{ij} and the singular values $\sigma_i(\mathbf{W})$, e.g., [23]–[25]. These weighted norms are defined as

$$\|\mathbf{A} \odot \mathbf{W}\|_1 = \sum_{i=1}^N \sum_{j=1}^K a_{ij} |w_{ij}|, \quad (4)$$

$$\|\mathbf{W}\|_{\mathbf{b},*} = \sum_{i=1}^{\operatorname{rank}(\mathbf{W})} b_i \sigma_i(\mathbf{W}), \quad (5)$$

where $a_{ij}, b_i \geq 0$ are weighting coefficients, which are explicitly defined in the next section. Utilizing (4) and (5), the proposed optimization problem is rewritten as

$$(P2) : \hat{\mathbf{W}} = \underset{\mathbf{W} \in \mathbb{R}_+^{N \times K}}{\operatorname{argmin}} \left\{ \frac{1}{2} \|\mathbf{Y} - \Phi \mathbf{W}\|_F^2 + \gamma \|\mathbf{A} \odot \mathbf{W}\|_1 + \tau \|\mathbf{W}\|_{\mathbf{b},*} \right\}. \quad (6)$$

To the best of our knowledge, a linear combination of a weighted ℓ_1 and a weighted nuclear norm, has not been used before as a regularizer for promoting simultaneously sparsity and low-rankness. Although convex, (P2) is a nontrivial problem to solve, due to the non-differentiable form of the ℓ_1 and nuclear norm regularizers, [26]. In the following, we utilize two standard convex optimization tools to tackle this problem; a proximal algorithm and an alternating direction method of multipliers (ADMM) based technique.

III. THE PROPOSED ALGORITHMS

In this section we present two methods to address the non-smooth, constrained, convex optimization problem in (P2). The first one is an incremental sub-gradient proximal method, [27], which makes use of the proximal operators of the regularizing terms in (P2), while the second, exploits the splitting strategy of an ADMM, [13].

A. Incremental proximal descent sparse and low-rank unmixing algorithm

From (P2) we define the following regularized quadratic loss function,

$$\mathcal{L}_1(\mathbf{W}) = \frac{1}{2} \|\mathbf{Y} - \Phi \mathbf{W}\|_F^2 + \gamma \|\mathbf{A} \odot \mathbf{W}\|_1 + \tau \|\mathbf{W}\|_{\mathbf{b},*} + 1_{\mathbb{R}_+}(\mathbf{W}), \quad (7)$$

where the nonnegativity constraint is now replaced by the indicator function $1_{\mathbb{R}_+}(\mathbf{W})$, which is zero when all $w_{ij} \geq 0, i = 1, 2, \dots, N, j = 1, 2, \dots, K$, and $+\infty$ if at least one w_{ij} is negative. Typically, we wish to minimize $\mathcal{L}_1(\mathbf{W})$ with respect to \mathbf{W} . Notice, however, that $\mathcal{L}_1(\mathbf{W})$ involves non-differentiable terms that require special attention. Hence, to minimize it, we deploy an incremental proximal method, introduced in [27], that considers separately the terms of the objective function.

Recall that the general definition of the proximal operator of a function $f(\cdot)$, [28], [29], is

$$\operatorname{prox}_{\lambda f}(v) = \underset{x}{\operatorname{argmin}} \left(f(x) + (1/2\lambda) \|x - v\|_2^2 \right), \quad (8)$$

where $v \in \mathbb{R}$ and $x \in \text{dom}(f)$. Next, we define the soft-thresholding operator on matrix $\mathbf{W} = [w]_{ij}$ as

$$\text{SHR}_{\Delta}(\mathbf{W}) = \text{sign}(\mathbf{W}) \max(\mathbf{0}, |\mathbf{W}| - \Delta), \quad (9)$$

where $\Delta = [\delta]_{ij}$ is the matrix that contains thresholding parameters. Note that the soft-thresholding in (9) is performed in an element-wise manner, i.e., $\text{SHR}_{\delta_{ij}}(w_{ij}) = \text{sign}(w_{ij}) \max(0, |w_{ij}| - \delta_{ij})$. Notably, when we apply the soft-thresholding operator on a diagonal matrix, we shrink only the elements belonging to its diagonal. These elements are assumed to be shrunk by thresholding parameters contained in a vector. With this in mind, we define the singular value thresholding operation by

$$\text{SVT}_{\delta}(\mathbf{W}) = \mathbf{U} \text{SHR}_{\delta}(\Sigma) \mathbf{V}^T$$

where $\mathbf{W} = \mathbf{U}\Sigma\mathbf{V}^T$ is the singular value decomposition (SVD) of \mathbf{W} , and δ is the vector whose entries are the thresholding parameters that reduce their corresponding diagonal elements of matrix Σ . Next, we define the following projection operator on the set of nonnegative real numbers,

$$\Pi_{\mathbb{R}_+}(v) = \arg \min_{x \in \mathbb{R}_+} |x - v| = \begin{cases} 0 & v < 0 \\ v & v \geq 0 \end{cases}, \quad (10)$$

which can also be applied to matrices, in an element-wise manner.

Utilizing the above definitions, we can compute the proximal operators for all regularizing terms in (7). First, the proximal operator of the nuclear norm can be expressed via a soft thresholding operation on the singular values of \mathbf{W} , i.e.,

$$\text{prox}_{\tau\|\cdot\|_{\mathbf{b},*}}(\mathbf{W}) = \text{SVT}_{\tau\mathbf{b}}(\mathbf{W}). \quad (11)$$

Similarly, $\text{prox}_{\gamma\|\mathbf{A}\odot\cdot\|_1}(\mathbf{W})$ is computed by soft-thresholding matrix \mathbf{W} with $\gamma\mathbf{A}$ as follows,

$$\text{prox}_{\gamma\|\mathbf{A}\odot\cdot\|_1}(\mathbf{W}) = \text{SHR}_{\gamma\mathbf{A}}(\mathbf{W}). \quad (12)$$

Moreover, the computation of $\text{prox}_{1_{\mathbb{R}_+}(\cdot)}(\mathbf{W})$ reduces to a projection operation, i.e.,

$$\text{prox}_{1_{\mathbb{R}_+}(\cdot)}(\mathbf{W}) = \Pi_{\mathbb{R}_+}(\mathbf{W}). \quad (13)$$

Algorithm 1 The proposed IPSpLRU algorithm

Inputs \mathbf{Y} , Φ

Select parameters τ, γ, η

Set $t = 0$, $\mathbf{R} = \Phi^T \Phi$, $\mathbf{P} = \Phi^T \mathbf{Y}$

Initialize \mathbf{W}^0

repeat

$$\mathbf{W}^t = \mathbf{W}^t - \eta (\mathbf{R}\mathbf{W}^t - \mathbf{P})$$

Update \mathbf{A}^t via eq. (15)

$$\mathbf{W}^t = \text{prox}_{\gamma \|\mathbf{A}^t \odot \cdot\|_1}(\mathbf{W}^t)$$

Update \mathbf{b}^t via eq. (15)

$$\mathbf{W}^t = \text{prox}_{\tau \|\cdot\|_{\mathbf{b}^t, *}}(\mathbf{W}^t)$$

$$\mathbf{W}^{t+1} = \text{prox}_{1_{\mathbb{R}_+}}(\cdot)(\mathbf{W}^t)$$

until convergence

Output : Abundance matrix $\hat{\mathbf{W}}$

Finally, the proximity operator of the differentiable Frobenius norm of the data fidelity term in (7) is equivalent to the following gradient step, [29],

$$\text{prox}_{\frac{\eta}{2} \|\mathbf{Y} - \Phi \cdot\|_F^2}(\mathbf{W}) = \mathbf{W} - \frac{\eta}{2} \nabla \|\mathbf{Y} - \Phi \mathbf{W}\|_F^2 = \mathbf{W} - \eta \Phi^T (\Phi \mathbf{W} - \mathbf{Y}), \quad (14)$$

where η is a positive stepsize parameter ².

The proposed incremental proximal sparse and low-rank unmixing algorithm (IPSpLRU) iterates among the proximal operators (14), (12), (11) and (13) in a cyclic order until convergence, [27]. Note that in (12) and (11) the weighted norms take the following (nonnegative) weight values,

$$a_{ij}^t = \left(\frac{1}{w_{ij}^t + \epsilon} \right) \text{ and } b_i^t = \left(\frac{1}{\sigma_i(\mathbf{W}^t) + \epsilon} \right), \quad (15)$$

where t is the iteration index and $\epsilon = 10^{-16}$ is a small constant added to avoid singularities. Similar weights have been used in [30] to form the matrix analogue of the adaptive lasso, [31]. IPSpLRU is summarized in Table 1.

²Actually eq. (14) holds approximately for small η 's

Concerning the computational complexity of IPSpLRU, the most complex step is the SVD of the abundance matrix \mathbf{W}^t , which takes place in each iteration and is of the order of $\mathcal{O}(KN^2 + K^3)$, [32]. When the endmembers' dictionary is ill-conditioned (which is a very usual situation in hyperspectral unmixing applications due to the high correlation of endmembers signatures), convergence of \mathbf{W}^t (from eq. (14)) is achieved when η is constrained to very small values. In such a framework, this leads to a slow convergence rate for IPSpLRU. To speed up convergence without compromising robustness, an ADMM-type scheme is presented next.

B. Alternating direction method of multipliers for sparse and low rank unmixing

In this section, we develop an instance of the alternating direction method of multipliers that solves the abundance matrix estimation problem given in (P2). As a rule, the ADMM considers the following augmented Lagrangian function, [13],

$$\begin{aligned} \mathcal{L}_2(\mathbf{W}, \Omega_1, \Omega_2, \Omega_3, \Omega_4) &= \frac{1}{2} \|\Omega_1 - \mathbf{Y}\|_F^2 + \gamma \|\mathbf{A} \odot \Omega_2\|_1 + \tau \|\Omega_3\|_{\mathbf{b},*} + 1_{\mathbb{R}_+}(\Omega_4) \\ &+ \text{tr} [\mathbf{D}_1^T (\Omega_1 - \Phi \mathbf{W})] + \text{tr} [\mathbf{D}_2^T (\Omega_2 - \mathbf{W})] + \text{tr} [\mathbf{D}_3^T (\Omega_3 - \mathbf{W})] + \text{tr} [\mathbf{D}_4^T (\Omega_4 - \mathbf{W})] \\ &+ \frac{\mu}{2} (\|\Phi \mathbf{W} - \Omega_1\|_F^2 + \|\mathbf{W} - \Omega_2\|_F^2 + \|\mathbf{W} - \Omega_3\|_F^2 + \|\mathbf{W} - \Omega_4\|_F^2) \end{aligned} \quad (16)$$

where the $L \times K$ matrix \mathbf{D}_1 , and the $N \times K$ matrices $\mathbf{D}_2, \mathbf{D}_3, \mathbf{D}_4$ are the Lagrange multipliers, and $\mu > 0$ is a positive penalty parameter. In addition, the weights \mathbf{A} and \mathbf{b} are computed as in the previous case. Let

$$\Omega = \begin{bmatrix} \Omega_1 \\ \Omega_2 \\ \Omega_3 \\ \Omega_4 \end{bmatrix}, \quad \mathbf{G} = \begin{bmatrix} \Phi \\ \mathbf{I}_N \\ \mathbf{I}_N \\ \mathbf{I}_N \end{bmatrix}, \quad \text{and } \mathbf{B} = \begin{bmatrix} -\mathbf{I}_L & \mathbf{0} & \mathbf{0} & \mathbf{0} \\ \mathbf{0} & -\mathbf{I}_N & \mathbf{0} & \mathbf{0} \\ \mathbf{0} & \mathbf{0} & -\mathbf{I}_N & \mathbf{0} \\ \mathbf{0} & \mathbf{0} & \mathbf{0} & -\mathbf{I}_N \end{bmatrix}. \quad (17)$$

Then (16) can be written in an equivalent form as

$$\begin{aligned} \mathcal{L}_3(\mathbf{W}, \Omega, \Lambda) &= \frac{1}{2} \|\Omega_1 - \mathbf{Y}\|_F^2 + \gamma \|\mathbf{A} \odot \Omega_2\|_1 + \tau \|\Omega_3\|_{\mathbf{b},*} \\ &+ 1_{\mathbb{R}_+}(\Omega_4) + \frac{\mu}{2} \|\mathbf{G}\mathbf{W} + \mathbf{B}\Omega - \Lambda\|_F^2, \end{aligned} \quad (18)$$

where $\Lambda = [\Lambda_1^T \ \Lambda_2^T \ \Lambda_3^T \ \Lambda_4^T]^T$, $\Lambda_i = (1/\mu)\mathbf{D}_i$, $i = 1, \dots, 4$, contains the scaled Lagrange multipliers. Having expressed the augmented Lagrangian function as in (18), the ADMM proceeds by minimizing $\mathcal{L}_3(\mathbf{W}, \Omega, \Lambda)$ sequentially, each time with respect to a single matrix variable, by

fixing the remaining variables at their latest values. The Lagrange multipliers are also updated at the end of each alternating minimization cycle.

To elaborate further on the steps of the ADMM, the optimization with respect to \mathbf{W} gives

$$\begin{aligned}\mathbf{W}^{t+1} &= \underset{\mathbf{W}}{\operatorname{argmin}} \mathcal{L}_3(\mathbf{W}, \Omega^t, \Lambda^t) \\ &= (\Phi^T \Phi + 3\mathbf{I}_N)^{-1} [\Phi^T (\Omega_1^t + \Lambda_1^t) + \Omega_2^t + \Lambda_2^t + \Omega_3^t + \Lambda_3^t + \Omega_4^t + \Lambda_4^t].\end{aligned}\quad (19)$$

Next, the optimization with respect to Ω_1 is performed as

$$\begin{aligned}\Omega_1^{t+1} &= \underset{\Omega_1}{\operatorname{argmin}} \mathcal{L}_3(\mathbf{W}^{t+1}, \Omega, \Lambda^t) \\ &= \frac{1}{1 + \mu} (\mathbf{Y} + \mu (\Phi \mathbf{W}^{t+1} - \Lambda_1^t)).\end{aligned}\quad (20)$$

The remaining auxiliary variables Ω_2, Ω_3 , and Ω_4 are involved in non-differentiable norms, namely, the weighted ℓ_1 norm, the weighted nuclear norm, and the indicator function, respectively. In this regard, the minimization task with respect to these variables resolves to computing some of the proximity operators that we introduced in the previous section. Minimizing (18) with respect to Ω_2 yields

$$\begin{aligned}\Omega_2^{t+1} &= \underset{\Omega_2}{\operatorname{argmin}} \mathcal{L}_3(\mathbf{W}^{t+1}, \Omega, \Lambda^t) \\ &= \operatorname{SHR}_{\gamma \mathbf{A}^t}(\mathbf{W}^{t+1} - \Lambda_2^t).\end{aligned}\quad (21)$$

In the same vein, Ω_3 is computed by a shrinkage operation,

$$\begin{aligned}\Omega_3^{t+1} &= \underset{\Omega_3}{\operatorname{argmin}} \mathcal{L}_3(\mathbf{W}^{t+1}, \Omega, \Lambda^t) \\ &= \operatorname{SVT}_{\tau \mathbf{b}^t}(\mathbf{W}^{t+1} - \Lambda_3^t).\end{aligned}\quad (22)$$

Next, for the auxiliary variable Ω_4 , a projection onto the nonnegative orthant is required,

$$\begin{aligned}\Omega_4^{t+1} &= \underset{\Omega_4}{\operatorname{argmin}} \mathcal{L}_3(\mathbf{W}^{t+1}, \Omega, \Lambda^t) \\ &= \Pi_{\mathbb{R}_+}(\mathbf{W}^{t+1} - \Lambda_4^t).\end{aligned}\quad (23)$$

At the final step of the proposed method, the scaled Lagrange multipliers in Λ are sequentially updated by performing gradient ascent on the dual problem [13], as follows,

$$\Lambda_1^{t+1} = \Lambda_1^t - \Phi \mathbf{W}^{t+1} + \Omega_1^{t+1}$$

$$\Lambda_i^{t+1} = \Lambda_i^t - \mathbf{W}^{t+1} + \Omega_i^{t+1}, i = 2, 3, 4 \quad (24)$$

The proposed algorithm, termed the alternating direction sparse and low-rank unmixing algorithm (ADSpLRU), is summarized in Algorithm 2. An iteration of ADSpLRU consists of the update steps given in (19), (20), (21), (22), (23), and (24). Its computational complexity is $\mathcal{O}(KLN + KN^2)$ per iteration, slightly higher than that of IPSpLRU, since usually it holds $L > N$. As verified by the simulations of the next section, ADSpLRU converges in a few iterations (around 40 to 60 depending on the problem), while its convergence is guaranteed as explained in [33].

Algorithm 2 The proposed ADSpLRU algorithm

Inputs \mathbf{Y}, Φ

Select parameters μ, τ, γ

Set $t = 0, \mathbf{R} = (\Phi^T \Phi + 3\mathbf{I}_N)^{-1}$

Initialize $\mathbf{W}^0, \Omega^0, \Lambda^0$

repeat

$$\mathbf{W}^{t+1} = \mathbf{R}[\Phi^T(\Omega_1^t + \Lambda_1^t) + \Omega_2^t + \Lambda_2^t + \Omega_3^t + \Lambda_3^t + \Omega_4^t + \Lambda_4^t]$$

$$\Omega_1^{t+1} = 1/(1 + \mu) (\mathbf{Y} + \mu (\Phi \mathbf{W}^{t+1} - \Lambda_1^t))$$

Update \mathbf{A}^t via eq. (15)

$$\Omega_2^{t+1} = \text{SHR}_{\gamma \mathbf{A}^t}(\mathbf{W}^{t+1} - \Lambda_2^t)$$

Update \mathbf{b}^t via eq. (15)

$$\Omega_3^{t+1} = \text{SVT}_{\tau \mathbf{b}^t}(\mathbf{W}^{t+1} - \Lambda_3^t)$$

$$\Omega_4^{t+1} = \Pi_{\mathbb{R}_+}(\mathbf{W}^{t+1} - \Lambda_4^t)$$

$$\Lambda_1^{t+1} = \Lambda_1^t - \Phi \mathbf{W}^{t+1} + \Omega_1^{t+1}$$

$$\Lambda_i^{t+1} = \Lambda_i^t - \mathbf{W}^{t+1} + \Omega_i^{t+1}, i = 2, 3, 4$$

until convergence

Output : Abundance matrix $\hat{\mathbf{W}} = \mathbf{W}^{t+1}$

IV. EXPERIMENTAL RESULTS

This section unravels the performance characteristics of the proposed IPSpLRU and ADSpLRU algorithms via experiments conducted both on simulated and real data. We compare our techniques with two well-known state-of-the-art ADMM based unmixing algorithms, namely,

TABLE I: Parameters Setting

Algorithm	τ (rank regularization parameter)	γ (sparsity regularization parameter)	μ
IPSpLRU	$\{0, e^{-10}, e^{-9}, \dots, e^{-1}\}$	$\{0, e^{-10}, e^{-9}, \dots, e^{-1}\}$	Not applicable
ADSpLRU	$\{0, e^{-10}, e^{-9}, \dots, e^{-1}\}$	$\{0, e^{-10}, e^{-9}, \dots, e^{-1}\}$	10^{-2}
CSUnSAL	Not applicable	$\{0, e^{-10}, e^{-9}, \dots, e^{-1}\}$	10^{-2}
MMV-ADMM	Not applicable	$\{0, e^{-10}, e^{-9}, \dots, e^{-1}\}$	10^{-2}

the nonnegative constraint sparse unmixing by variable splitting and augmented Lagrangian algorithm (CSUnSAL), [5], and the recently reported nonnegative constraint joint-sparse method (MMV-ADMM), [10]. In what follows, we first refer to the parameters' setting established for all the involved algorithms, and the performance evaluation metrics that are utilized in the experimental procedure. To corroborate the effectiveness and the robustness of the proposed algorithms we execute four different types of synthetic data experiments whose detailed description is given below. Finally, we empirically compare the abundance maps as revealed by all examined algorithms, when applied on a real hyperspectral image.

A. Setting of Parameters and Performance Evaluation Criteria

For simplicity reasons, we use γ for the sparsity imposing parameter in all tested algorithms, and μ for the Lagrange multiplier regularization parameter of the ADMM-type techniques. Additionally, the low-rank promoting parameter of the proposed algorithms, is denoted by τ . Parameters τ and γ are fine tuned with 10 different values, as shown in Table 1. On the other hand, the Lagrange multiplier regularization parameter μ , which influences to a less extend the efficiency of the corresponding algorithms, is set to a fixed value. In order to assess the performance of the proposed algorithms and the competing ones, for the experiments conducted on synthetic data we consider two metrics. First, the root mean square error (RMSE),

$$\text{RMSE} = \sqrt{\frac{1}{Nn} \sum_{i=1}^n \|\hat{\mathbf{w}}_i - \mathbf{w}_i\|_2}, \quad (25)$$

where $\hat{\mathbf{w}}_i$ and \mathbf{w}_i represent the estimated and actual abundance vectors of the i -th pixel respectively, n is the number of the pixels, and N , as mentioned in previous sections, stands for

the number of endmembers. The second metric, is the signal-to-reconstruction error (SRE), [6], which reflects the ratio between the power of the signal and the power of the estimation error, and is given by the following formula

$$\text{SRE} = 10\log_{10} \left(\frac{\frac{1}{n} \sum_{i=1}^n \|\hat{\mathbf{w}}_i\|_2^2}{\frac{1}{n} \sum_{i=1}^n \|\hat{\mathbf{w}}_i - \mathbf{w}_i\|_2^2} \right). \quad (26)$$

Of great importance is to notice that for the window-based algorithms, the abundance vectors \mathbf{w}_i 's and their estimates $\hat{\mathbf{w}}_i$'s coincide with the central column vectors of the corresponding abundance matrices \mathbf{W}_i 's and their estimates $\hat{\mathbf{W}}_i$'s, as becomes clear from Fig. 1.

B. Experiments on Simulated Datacubes

In the sequel, $N = 25$ endmembers are randomly selected from the USGS library $\mathbf{Q} \in \mathbb{R}_+^{224 \times 498}$, [34], so as to form our endmembers' dictionary Φ . Their reflectance values correspond to 224 spectral bands, uniformly distributed in the interval $0.4 - 2.5\mu m$. The LMM of eq. (1) is then utilized for generating spectral signatures subject to given, different in each experiment, abundance matrices \mathbf{W} 's.

1) *A toy example:* In this experiment our goal is to highlight the significance of the approach followed in this work, i.e., the simultaneous incorporation of sparsity and low-rankness on the abundance estimation problem. To this end, we initially derive the single prior counterparts of our algorithms. We first focus on the low-rankness assumption, thus the sparsity imposing norm is ignored ($\gamma = 0$). IPSpLRU and ADSpLRU are then reduced to their modified versions, namely, IPLRU and ADLRU respectively. As implied by their names, the aforementioned methods allow exclusively for the low-rank assumption. Similarly, IPSpU and ADSpU are formed by accounting solely for sparsity. That said, IPSpU and ADSpU emerge after dropping the low-rank prior constraint ($\tau = 0$). Next, we generate a $N \times K$ (where $K = 9$) simultaneously sparse and low-rank abundance matrix \mathbf{W} of rank 2 and with sparsity level 20% (i.e., 20% of the entries of \mathbf{W} are nonzero), which is graphically illustrated in Fig. 2a. Using this \mathbf{W} we generate via the LMM in eq. 1, where \mathbf{E} is Gaussian i.i.d noise of SNR=35dB.

Fig. 2 shows the merits of the proposed IPSpLRU and ADSpLRU algorithms. Specifically, it appears that the concurrent exploitation of sparsity and low-rankness, leads to significantly more accurate abundance matrix estimates, as compared to their single constraint counterparts, namely, IPLRU, IPSpU and ADLRU, ADSpU respectively. This is clearly seen both in terms

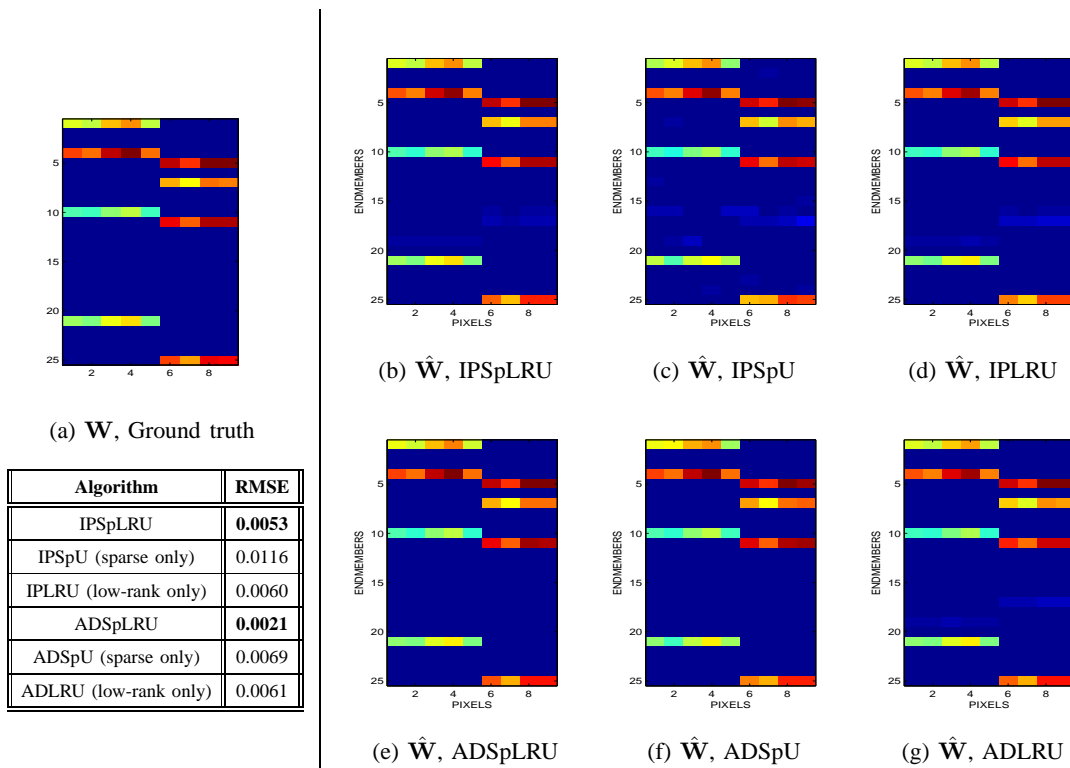


Fig. 2: Sparse and low-rank algorithms versus their sparse only and low-rank only counterparts.

of the RMSE and a careful visual inspection of the recovered abundance matrices, depicted in Figs. 2b - 2g.

2) *The key role of the parameters γ, τ* : As explained earlier, parameters γ and τ control the imposition of sparsity and low-rankness, respectively, on the abundance matrix \mathbf{W} . Herein, we unveil the dependency of the optimal (with respect to RMSE minimization) set of these parameters on the inherent structure of the sought abundance matrix. In this vein, three different types of abundance matrices are generated, each reflecting a specific combination of rank and sparsity level. Next, $K = 9$ linearly mixed pixels are produced, corrupted with Gaussian i.i.d noise of SNR=35dB. As shown in Fig. 3, in all examined cases RMSE is minimized at the inner region of the grid formed by the different values of the parameters τ, γ (i.e. both $\tau \neq 0$ and $\gamma \neq 0$). Moreover, it is illustrated that the optimal set of τ, γ is subject to the sparsity level and rank of the corresponding abundance matrix. This gives us good grounds for emphasizing on the

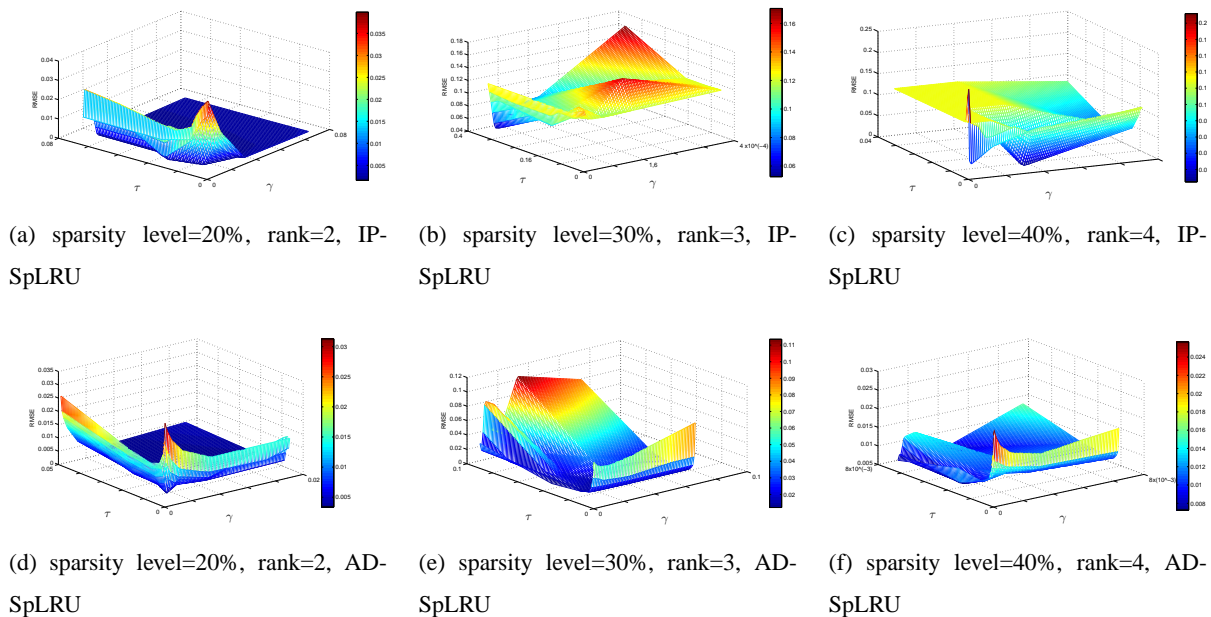


Fig. 3: RMSE as a function of the low-rankness and the sparsity regularization parameters τ and γ , respectively.

need for a proper selection of their values. By all means, this choice should take into account our intuition concerning the structure of the latent abundance matrix.

3) *Robustness to noise*: In this experiment we aim at exhibiting the robustness of the proposed algorithms to white and correlated noise corruption. To this end, we stick with a specific simultaneously sparse and low-rank abundance matrix \mathbf{W} of sparsity level 20% and rank 3. Based on this \mathbf{W} , $K = 9$ linearly mixed pixels are generated, in the same way as described above. Then, depending on the case, white or colored Gaussian noise contaminates the data. 16 SNR values are considered ranging from 10 to 40 dB, while 50 realizations are run for each SNR value, and the mean of the RMSE and SRE metrics is calculated.

- *White Gaussian Noise*: Fig. 4 shows the RMSE and SRE curves obtained for the proposed IPSpLRU, ADSpLRU and the two competing algorithms, namely, CSUnSAL and MMV-ADMM. It is easily seen that both IPSpLRU and ADSpLRU attain remarkably better results comparing to CSUnSAL and MMV-ADMM, in all the examined SNR values. Additionally, we note that IPSpLRU performs slightly better as compared to ADSpLRU, for SNR values greater than 22dB. The price to be paid, is that IPSpLRU requires much more iterations

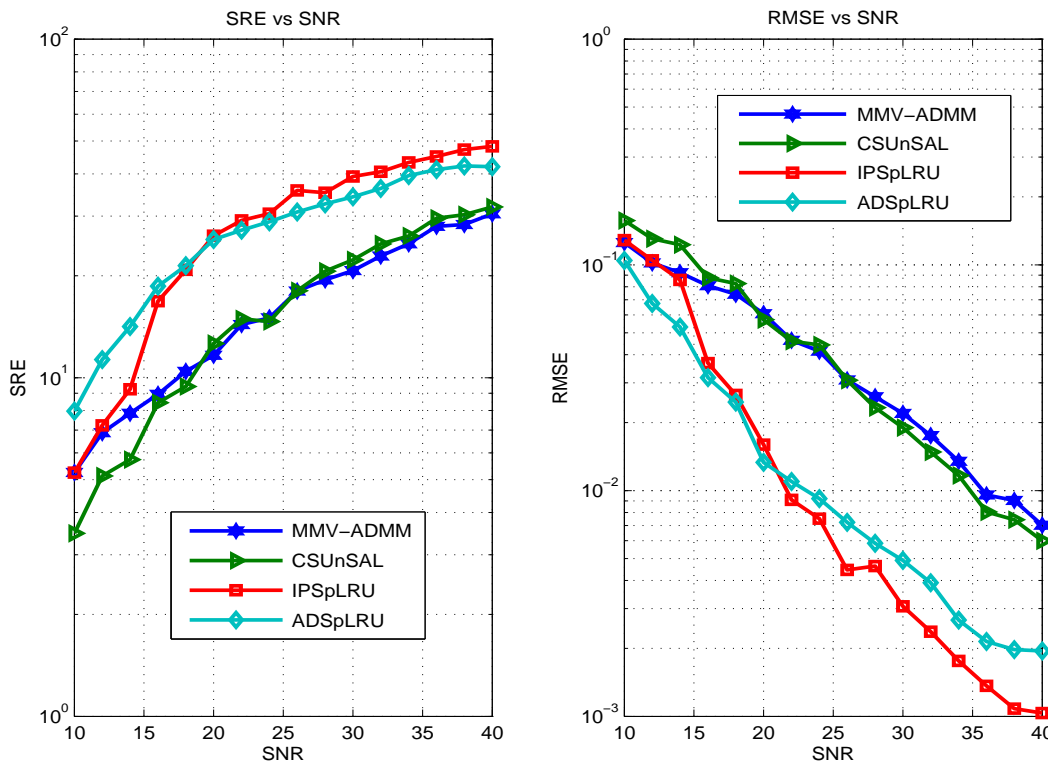


Fig. 4: Robustness to white noise (SRE & RMSE).

to converge, in contrast to ADSpLRU which converges very fast in a few iterations. It is hence shown, that sparse and low-rank methods are robust to different levels of white noise. At the same time, IPSpLRU and ADSpLRU outperform the sparse only CSUnSAL and the joint-sparse MMV-ADMM algorithms, provided that both sparsity and low-rankness characterizes the abundance matrix.

- *Colored Gaussian Noise:* Actually, in real hyperspectral images the noise that corrupts the data is rather structured than white. Thus, to assess the behavior of the proposed methods in such realistic conditions, we simulate correlated Gaussian noise that adds up to the linearly mixed pixels. Fig. 5 illustrates the effectiveness of the tested algorithms in terms of RMSE and SRE, for different SNR values. Therein as well, we can see that IPSpLRU and ADSpLRU achieve better results than their competing algorithms in the whole range of the examined SNRs. Furthermore, IPSpLRU performs better for all the SNR values, as

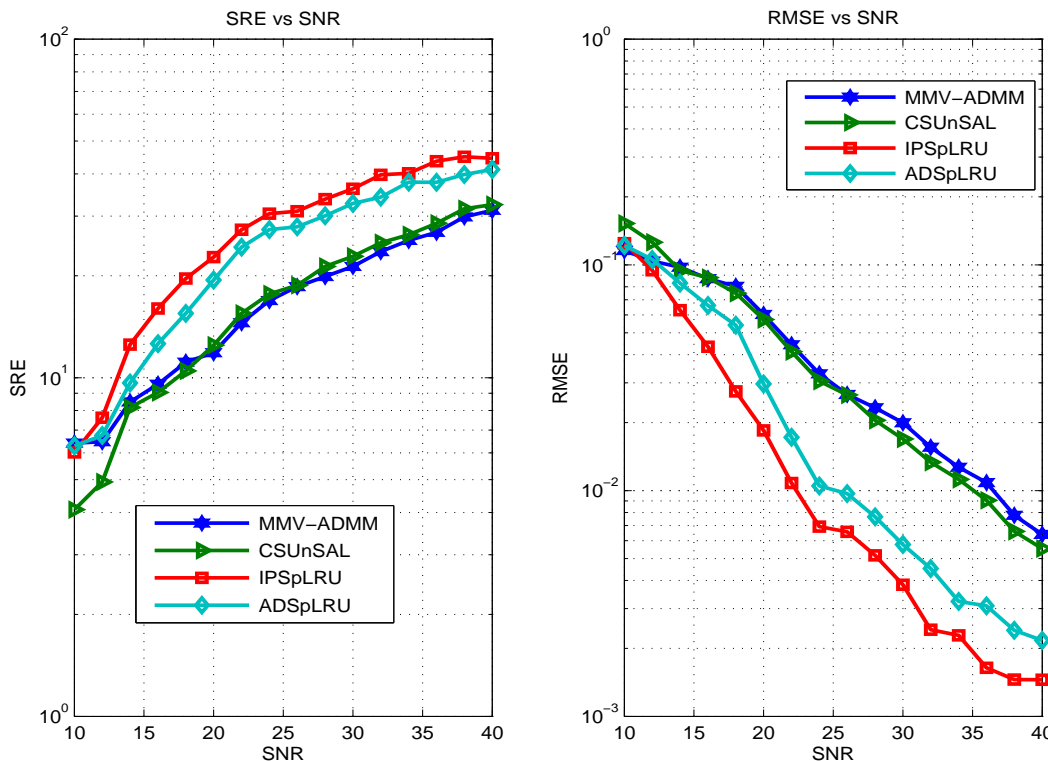


Fig. 5: Robustness to colored noise (SRE & RMSE).

compared to ADSpLRU. As a result, the robustness of our proposed methods is corroborated in the presence of correlated noise with different magnitude.

4) *Synthetic Image*: This experiment highlights the effectiveness of the proposed methods in estimating sparse, low-rank or both sparse and low-rank abundance matrices. On this purpose we form a simulated hyperspectral image using the linear mixing model (1) and the same above-mentioned endmembers' dictionary Φ . As shown in Fig. 6a, the simulated hyperspectral image consists of 4 rows each consisting of 2 10×10 blocks of pixels. Each of the “block rows” is generated by abundance matrices of a distinct structure. To be more specific, the first row is generated by joint-sparse \mathbf{W} 's, the second by solely low-rank \mathbf{W} 's while rows 3 and 4 are produced by simultaneously sparse and low-rank abundance matrices. The pixels in each block correspond to abundance matrices of a particular combination of sparsity level and rank. The detailed description of these structures is depicted in the table of Fig. 6b. The linearly mixed

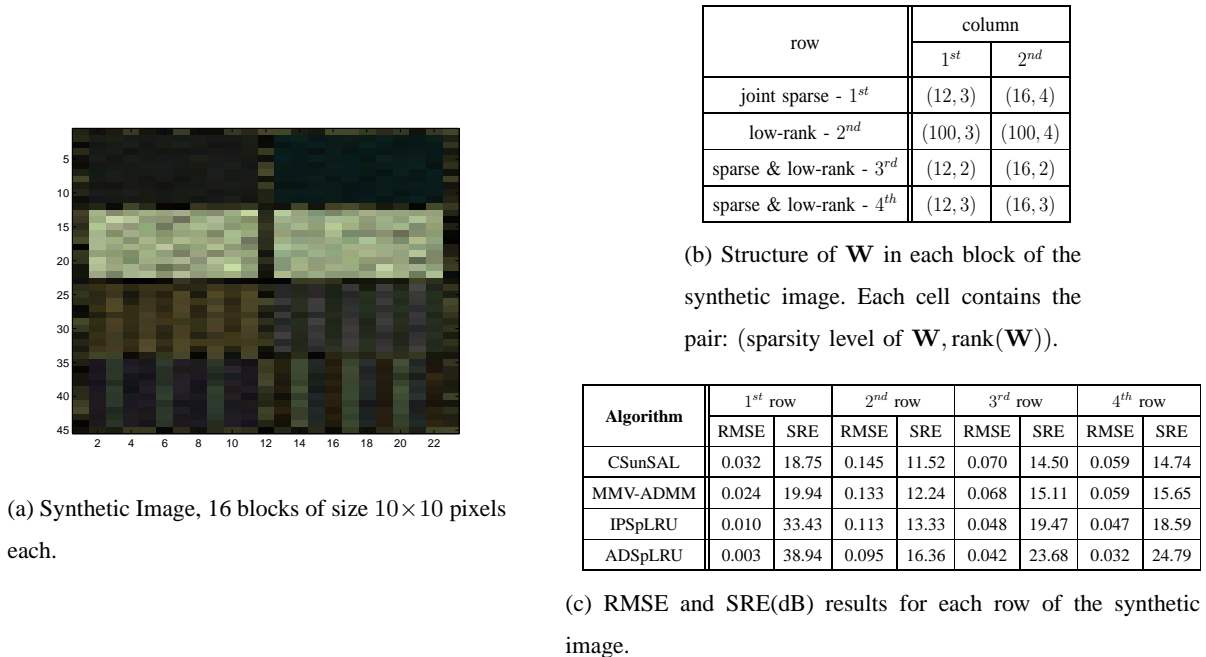


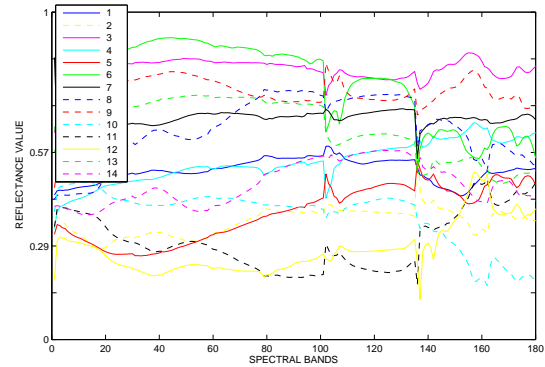
Fig. 6: Synthetic image and results.

pixels are corrupted by white Gaussian i.i.d noise of SNR = 30dB. The table in Fig. 6c contains the obtained RMSE and SRE for all algorithms tested. It is worth pointing out that our introduced IPSpLRU and ADSpLRU algorithms outperform their rivals, not only in the “both sparse and low-rank” rows 3 and 4, but also in rows 1 and 2 that correspond to either sparse only or low-rank only \mathbf{W} 's.

C. Experiment on Real Data

This section illustrates the performance of the proposed algorithms when applied on a real hyperspectral image. The hyperspectral scene under examination is the widely used AVIRIS Cuprite image captured over the Cuprite mining region in NV, USA. The Cuprite dataset is available on-line in reflectance units³. In this experiment we selected a subregion of size 75×100 pixels, of the sector labeled as “f970619t01p02_r02_sc03.a.rf” in the on-line dataset. This scene consists of 224 spectral bands distributed between 0.4 and 2.5 μm , with a nominal spectral resolution of 10nm. Due to water absorption and low SNR values, bands 1-2, 105-115, 150-170

³<http://aviris.jpl.nasa.gov/html/aviris.freedata.html>



(a) False color illustration of sector “f970619t01p02_r02_sc03.a.rf” of the Cuprite region. The region we examine is included in the black box. (b) Spectral signatures of the 14 endmembers extracted by the MVSA method, from the sector “f970619t01p02_r02_sc03.a.rf”.

Fig. 7: Cuprite image and endmembers’ dictionary

and 223-224 are removed. Hence, 188 spectral bands are left. A false color illustration of the whole sector and our examined region is shown in Fig. 7a.

In the first step, the geometrical endmembers’ extraction algorithm termed as minimum volume simplex analysis (MVSA) of [3] is applied on the whole sector of the Cuprite dataset. MVSA assumes linearly mixed pixels, and is able to extract the spectral signatures of the endmembers, even in cases that the pure pixels assumption is violated. This characteristic has been proven to lead to estimates of higher accuracy as compared to the pure pixel based methods. As is known, 14 endmembers that reflect different minerals, lie in the sector “f970619t01p02_r02_sc03.a.rf” of the Cuprite image, where our region of interest lies. To this end, we properly parameterize the MVSA algorithm so as to build our dictionary with 14 endmembers signatures, displayed in Fig. 7b.

Fig. 8 shows the abundance maps corresponding to the region of our interest, as obtained by the proposed IPSpLRU, ADSpLRU and the two state-of-the-art competing algorithms namely CSUnSAL and MMV-ADMM for $\gamma = 10^{-3}$, $\tau = 10^{-4}$ and $\mu = 10^{-2}$. It is worth pointing out that since ground truth is not available, the evaluation can be done only in qualitative terms. From

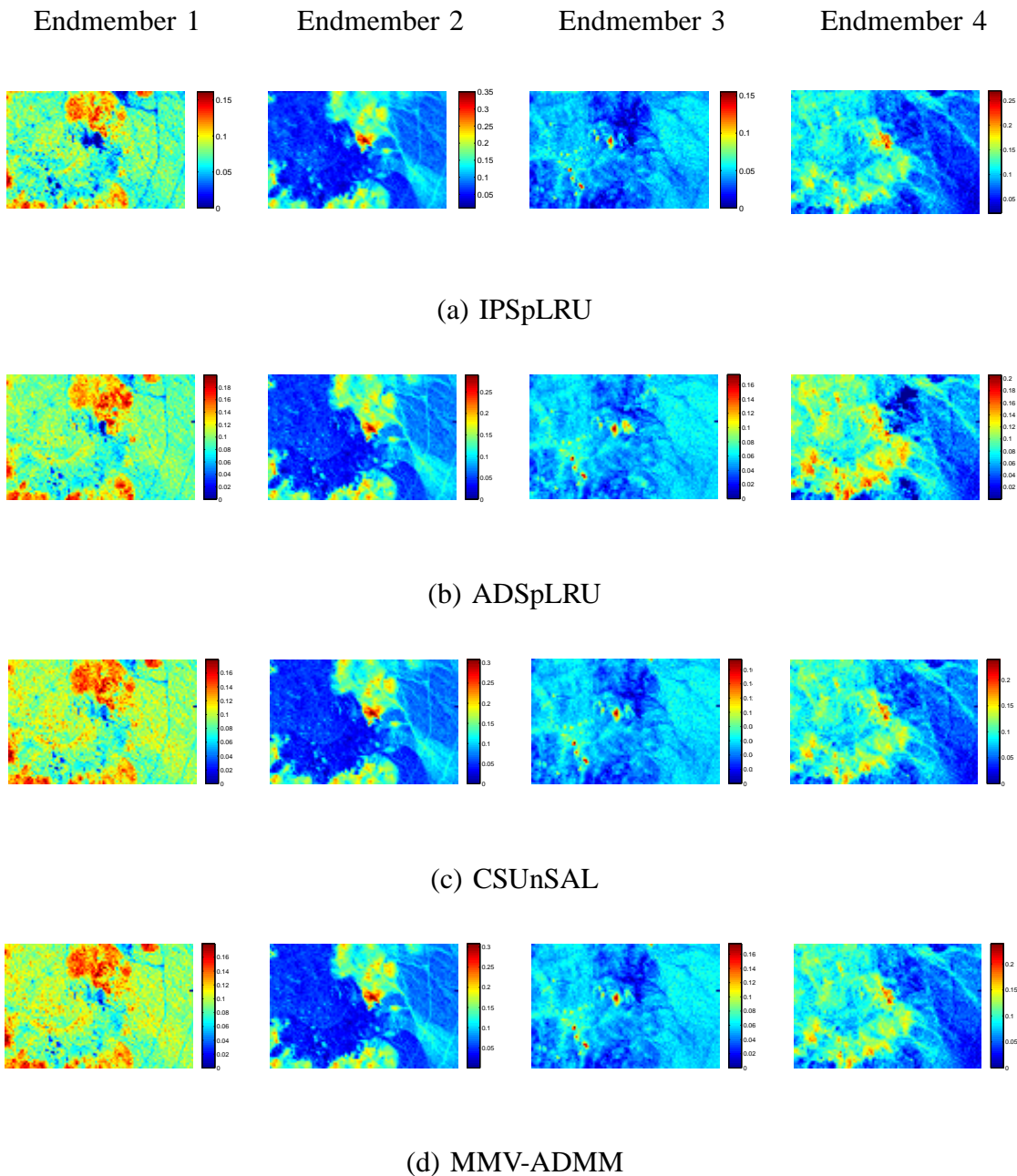


Fig. 8: Abundance maps of a subregion of the Cuprite hyperspectral image.

a careful visual inspection of the generated maps, we can see that all the algorithms produce similar patterns. Since no ground truth is available comparisons are limited, and a more analytical validation is not possible. Nevertheless, these results confirm that the proposed algorithms work

well and provide reasonable and meaningful abundance maps of materials existing in a real hyperspectral image.

V. CONCLUSIONS AND FUTURE DIRECTIONS

In this paper we presented a novel approach for performing hyperspectral image unmixing exploiting simultaneously sparsity and spatial correlation. A novel convex cost function was first introduced comprising a least squares proximity component regularized by a linear combination of the weighted ℓ_1 and the weighted nuclear norm of the latent abundance matrix. The unmixing problem was thus treated as a sparse reduced-rank regression problem. Two different algorithms were then developed for solving it, namely an incremental proximal type algorithm called IPSpLRU, and an ADMM based strategy called ADSpLRU. Extensive simulations on both synthetic and real data corroborate the effectiveness of proposed approach and algorithms, compared to other related state-of-the-art unmixing schemes. The derivation of more computationally efficient schemes alleviating the need for SVD is under current investigation. Another relevant research direction is the exploitation of the specific structure or pattern of sparsity in the abundance matrices imposed implicitly by the low-rankness property, which could further improve estimation performance. This is also a topic of interest in the framework of a future work.

REFERENCES

- [1] W. Ma, J. Bioucas-Dias, T.-H. Chan, N. Gillis, P. Gader, A. Plaza, A. Ambikapathi, and C.-Y. Chi, "A signal processing perspective on hyperspectral unmixing: insights from remote sensing," *Signal Processing Magazine, IEEE*, vol. 31, no. 1, pp. 67–81, Jan. 2014.
- [2] J. Nascimento and J. Bioucas-Dias, "Vertex component analysis: a fast algorithm to unmix hyperspectral data," *Geoscience and Remote Sensing, IEEE Transactions on*, vol. 43, no. 4, pp. 898–910, April 2005.
- [3] J. Li and J. Bioucas-Dias, "Minimum volume simplex analysis: a fast algorithm to unmix hyperspectral data," in *Geoscience and Remote Sensing Symposium (IGARSS). IEEE International*, vol. 3, July 2008, pp. III – 250–III – 253.
- [4] K. E. Themelis, A. A. Rontogiannis, and K. D. Koutroumbas, "Semi-supervised hyperspectral unmixing via the weighted lasso," in *Acoustics, Speech and Signal Processing (ICASSP), IEEE International Conference on*, March 2010, pp. 1194–1197.
- [5] J. Bioucas-Dias and M. Figueiredo, "Alternating direction algorithms for constrained sparse regression: application to hyperspectral unmixing," in *Hyperspectral Image and Signal Processing: Evolution in Remote Sensing (WHISPERS), 2nd Workshop on*, June 2010, pp. 1–4.
- [6] M.-D. Iordache, J. Bioucas-Dias, and A. Plaza, "Sparse unmixing of hyperspectral data," *Geoscience and Remote Sensing, IEEE Transactions on*, vol. 49, no. 6, pp. 2014–2039, June 2011.

- [7] K. E. Themelis, A. A. Rontogiannis, and K. D. Koutroumbas, “A novel hierarchical Bayesian approach for sparse semi-supervised hyperspectral unmixing,” *Signal Processing, IEEE Transactions on*, vol. 60, no. 2, pp. 585–599, Feb. 2012.
- [8] A. A. Rontogiannis, K. E. Themelis, and K. D. Koutroumbas, “A fast variational Bayes algorithm for sparse semi-supervised unmixing of Omega/Mars express data,” in *Hyperspectral Image and Signal Processing: Evolution in Remote Sensing (WHISPERS), 5th Workshop on*, June 2013, pp. 974–978.
- [9] O. Eches, N. Dobigeon, and J.-Y. Tourneret, “Enhancing hyperspectral image unmixing with spatial correlations,” *Geoscience and Remote Sensing, IEEE Transactions on*, vol. 49, no. 11, pp. 4239–4247, Nov. 2011.
- [10] Q. Qu, N. Nasrabadi, and T. Tran, “Abundance estimation for bilinear mixture models via joint sparse and low-rank representation,” *Geoscience and Remote Sensing, IEEE Transactions on*, vol. 52, no. 7, pp. 4404–4423, July 2014.
- [11] M.-D. Iordache, J. Bioucas-Dias, and A. Plaza, “Collaborative sparse regression for hyperspectral unmixing,” *Geoscience and Remote Sensing, IEEE Transactions on*, vol. 52, no. 1, pp. 341–354, Jan. 2014.
- [12] P. V. Giampouras, K. E. Themelis, A. A. Rontogiannis, and K. D. Koutroumbas, “A variational Bayes algorithm for joint-sparse abundance estimation,” in *Hyperspectral Image and Signal Processing: Evolution in Remote Sensing (WHISPERS), 6th Workshop on*, June 2014.
- [13] S. Boyd, N. Parikh, E. Chu, B. Peleato, and J. Eckstein, “Distributed optimization and statistical learning via the alternating direction method of multipliers,” *Foundations and Trends® in Machine Learning*, vol. 3, no. 1, pp. 1–122, 2011.
- [14] L. Chen and J. Z. Huang, “Sparse reduced-rank regression for simultaneous dimension reduction and variable selection,” *Journal of the American Statistical Association*, vol. 107, no. 500, pp. 1533–1545, 2012.
- [15] P.-A. Savalle, E. Richard, and N. Vayatis, “Estimation of simultaneously sparse and low rank matrices,” in *International Conference on Machine Learning (ICML)*, June 2012.
- [16] S. Oymak, A. Jalali, M. Fazel, Y. C. Eldar, and B. Hassibi, “Simultaneously structured models with application to sparse and low-rank matrices,” *arXiv preprint arXiv:1212.3753*, 2012.
- [17] M. Golbabaee and P. Vandergheynst, “Compressed sensing of simultaneous low-rank and joint-sparse matrices,” *arXiv preprint arXiv:1211.5058*, 2012.
- [18] N. Keshava and J. F. Mustard, “Spectral unmixing,” *Signal Processing Magazine, IEEE*, vol. 19, no. 1, pp. 44–57, 2002.
- [19] S. Negahban and M. J. Wainwright, “Estimation of (near) low-rank matrices with noise and high-dimensional scaling,” *The Annals of Statistics*, vol. 39, no. 2, pp. 1069–1097, April 2011.
- [20] S. Babacan, M. Luessi, R. Molina, and A. Katsaggelos, “Sparse Bayesian methods for low-rank matrix estimation,” *Signal Processing, IEEE Transactions on*, vol. 60, no. 8, pp. 3964–3977, Aug. 2012.
- [21] F. R. Bach, “Consistency of trace norm minimization,” *Journal of Machine Learning Research*, vol. 9, pp. 1019–1048, June 2008.
- [22] W. Tang, Z. Shi, Y. Wu, and C. Zhang, “Sparse unmixing of hyperspectral data using spectral a priori information,” *Geoscience and Remote Sensing, IEEE Transactions on*, vol. 53, no. 2, pp. 770–783, Feb. 2015.
- [23] C. Lu, J. Tang, S. Yan, and Z. Lin, “Generalized nonconvex nonsmooth low-rank minimization,” *arXiv preprint arXiv:1404.7306*, 2014.
- [24] E. J. Candes, M. B. Wakin, and S. P. Boyd, “Enhancing sparsity by reweighted L1 minimization,” *Journal of Fourier Analysis and Applications*, vol. 14, no. 5-6, pp. 877–905, 2008.
- [25] Y.-D. Kim and S. Choi, “Variational Bayesian view of weighted trace norm regularization for matrix factorization,” *Signal Processing Letters, IEEE*, vol. 20, no. 3, pp. 261–264, March 2013.

- [26] F. Bach, R. Jenatton, J. Mairal, G. Obozinski *et al.*, “Convex optimization with sparsity-inducing norms,” *Optimization for Machine Learning*, pp. 19–53, 2011.
- [27] D. P. Bertsekas, “Incremental gradient, subgradient, and proximal methods for convex optimization: a survey,” *Optimization for Machine Learning*, vol. 2010, pp. 1–38, 2011.
- [28] P. L. Combettes and J.-C. Pesquet, “Proximal splitting methods in signal processing,” in *Fixed-point algorithms for inverse problems in science and engineering*. Springer, 2011, pp. 185–212.
- [29] N. Parikh and S. Boyd, “Proximal algorithms,” *Foundations and Trends in Optimization*, vol. 1, no. 3, pp. 123–231, 2013.
- [30] J. Bien and R. J. Tibshirani, “Sparse estimation of a covariance matrix,” *Biometrika*, vol. 98, no. 4, pp. 807–820, 2011.
- [31] H. Zou, “The adaptive lasso and its oracle properties,” *Journal of the American Statistical Association*, vol. 101, no. 476, pp. 1418–1429, 2006.
- [32] G. H. Golub and C. F. Van Loan, *Matrix Computations*. JHU Press, 2012.
- [33] J. Eckstein and D. P. Bertsekas, “On the Douglas-Rachford splitting method and the proximal point algorithm for maximal monotone operators,” *Mathematical Programming*, vol. 55, no. 1-3, pp. 293–318, 1992.
- [34] R. N. Clark, G. A. Swayze, R. Wise, K. E. Livo, T. M. Hoefen, R. F. Kokaly, and S. J. Sutley, “USGS digital spectral library,” 2007, <http://speclab.cr.usgs.gov/spectral.lib06/ds231/datatable.html>.